Refereed Proceedings

The 12th International Conference on Fluidization - New Horizons in Fluidization Engineering

Engineering Conferences International *Year* 2007

Homogeneous to Bubbling Regime Transition in Gas- and Liquid-Fluidized Beds Through DEM-CFD Simulations

Alberto Di Renzo* Francesco P. Di Maio†

*Università della Calabria, Italy, alberto.direnzo@unical.it

†Università della Calabria, Italy

HOMOGENEOUS TO BUBBLING REGIME TRANSITION IN GAS- AND LIQUID-FLUIDIZED BEDS THROUGH DEM-CFD SIMULATIONS

Alberto Di Renzo and Francesco P. Di Maio
Dipartimento di Ingegneria Chimica e dei Materiali
Università della Calabria, Via P. Bucci Cubo 44A, 87036 Rende (CS)
T: +39 0984 496654; F: +39 0984 496655; E: alberto.direnzo@unical.it

ABSTRACT

DEM-CFD simulations are carried out for the water fluidization of 200 μm glass ballotini and air fluidization of cohesionless alumina 70 μm powders. In the first case, homogeneous expansion is found throughout the whole investigated range of water velocity. Alumina powders exhibits a transition to bubbling regime at a voidage value in very good agreement with results of the theory of particle bed stability. The simulated kinematic and dynamic wave propagation velocities are in good agreement with theoretical predictions.

INTRODUCTION

Computational techniques based on the Distinct Element Method (DEM, (1)) and CFD for the fluid flow calculations have allowed significant aspects of the fluidization patterns of complex systems to be reproduced with remarkable accuracy. The coupled DEM-CFD approach is very CPU intensive and simulations of large systems are, if possible, still extremely time demanding. On the other hand, given its first principles and small scale modelling approach, it proved an unparallel power and versatility in studying the fundamental aspects of the fluidization science.

In the literature, while in the majority of papers where the DEM-CFD approach was used bubbling fluidization is simulated and analysed, very few of them deal with homogeneous gas-fluidization and, to the authors' knowledge, the propagation of voidage shocks and waves has not been addressed yet. As it is well known, these are responsible for the transition from the homogeneous expansion to the bubbling regime in Group A powders when particle-particle cohesive forces are negligible. Even in the presence of cohesive forces, the fluid-dynamic action on the suspension is crucial and deserves a particular importance in understanding and predicting the bed behaviour of gas-particle systems. As far as liquid-fluidized beds are concerned, preliminary results of DEM simulations have been recently obtained by Malone et al. (2). Earlier, liquid-particle interactions have been considered in the context of the analysis of gas bubble formation in a gas-liquid-solid system (see e.g. (3)). Regarding simulations of the air-fluidization of fine powders (Geldart's Group A) Ye et al. (4) found homogeneous expansion behaviour and studied the effect of the superposition

The 12th International Conference on Fluidization - New Horizons in Fluidization Engineering, Art. 81 [2007]

of an inter-particle cohesive force. Qualitative characterization of the competing mechanisms in determining the regime was performed. The same authors in a later work (5) compared the determination of minimum bubbling conditions through DEM–CFD simulations with the results obtained using well-established correlations. The effect of the physical properties of the gas and the particles on u_{mb} showed good agreement for nearly all the properties investigated. Similarly, Pandit et al. (6) used DEM–CFD simulations to study the expansion behaviour of Geldart's Group A particles with and without an imposed cohesive force. The simulated particles were located near the Group A/B borderline and the issue of homogeneous stability related to voidage waves was only referred to during the discussion of the results and no attempt was made to characterise it quantitatively.

In the present paper, we illustrate DEM-CFD simulations of the fluidization regime established in two systems at various fluid velocities in order to assess the capability of the approach to capture the essential fluid-particle interactions and be able to reproduce the correct bed behaviour in the different cases. To this purpose, simulations of the behaviour of a system consisting of glass beads fluidized by water will be considered, together with the gas-fluidization of Geldart's Group A particles. In the former case, the fluid-particle interactions are treated in a simplified manner, since only drag and pressure gradient forces on the particles will be considered. However, the phenomena are analysed under conditions ensuring that contributions arising in accelerating motion of particles (e.g. added mass, history integral forces and others) can be safely neglected. The numerical simulations will be considered in the context of the general stability theory of the fluidized bed state developed by Foscolo and Gibilaro (7), known as the Particle Bed Model. Within this framework, the propagation of voidage waves along the suspension will also be addressed as further means of validation of the DEM–CFD approach.

MODEL EQUATIONS

The model formulation follows the conventional DEM-CFD set of equations available in literature. The key points will be summarized here, concentrating on the peculiar aspects of the whole modelling procedure and neglecting the details whenever possible. Newton's second law of dynamics is solved for each particle in the system

$$m\mathbf{a} = m\mathbf{g} + \sum_{j=1}^{nC} \mathbf{f}_{c,j} + \mathbf{f}_d - \nabla p V_p \tag{1}$$

where the gravitational, contact, drag and pressure gradient forces are considered. Contact forces are calculated using a soft-sphere non-linear force-displacement law presented elsewhere (8). The drag formulas are as developed by Di Felice (9)

$$\mathbf{f}_d = \tfrac{1}{2} C_D \, \rho \pi R^2 \, \varepsilon^2 \left|\mathbf{u} - \mathbf{v}\right|\left(\mathbf{u} - \mathbf{v}\right) \cdot \varepsilon^{-\chi} \tag{2}$$

$$\chi = 3.7 - 0.65 \cdot \exp\left[-\frac{\left(1.5 - \log_{10} \mathrm{Re}_p\right)^2}{2} \right] \tag{3}$$

Accordingly, the continuity and momentum balance equations governing the motion of

the continuous fluid phase are

$$\frac{\partial \rho \varepsilon}{\partial t} + \nabla \cdot \rho \varepsilon \mathbf{u} = 0 \tag{4}$$

$$\frac{\partial \rho \varepsilon \mathbf{u}}{\partial t} + \nabla \cdot \rho \varepsilon \mathbf{u}\mathbf{u} = -\varepsilon \nabla p + \nabla \cdot \boldsymbol{\tau} + \mathbf{F}_{fp} + \rho \varepsilon \mathbf{g} \tag{5}$$

where

$$\mathbf{F}_{fp} = -\frac{\sum_{i=1}^{nP} \mathbf{f}_{d,i}}{\Omega} \tag{6}$$

While Eqs. (4) and (5) are written in terms of local variables, in Eq. (6) the (finite) volume Ω appears explicitly. In fact, in the derivation of a discretized form of the equations to be solved numerically, the continuity and Navier-Stokes equations are written in integral form on a control volume, following the so called *finite volume method*. On this issue, it is noteworthy that the definition of “voidage” as a fractional occupation of volume by the fluid phase implies a finite volume to be considered as a basis. Otherwise, in a *local* frame of reference, unity and zero voidage values would result in spatial points located outside and inside particles, respectively.

LIQUID-FLUIDIZED BED

Despite the simplicity of the expansion regime characterising beds fluidized by a liquid, in the literature, to the authors' knowledge, there is only one attempt to use DEM–CFD simulations to represent their behaviour (2). As will be shown in the following subsections, the time-scale of dynamic phenomena is by an order of magnitude larger than in gas-fluidized systems. Therefore, longer simulations are required in order to analyse the dynamic response of a fluidized bed to a change in the operating parameters and to achieve steady-state conditions. Moreover, from a numerical point of view, convergence in the fluid phase solution is more difficult to obtain and a large number of iterations is necessary in order to reach a solution. As a consequence, the campaign of simulations will not be as extensive as for gas-fluidized beds.

The systems considered consists of a pseudo-2D geometry where 15000 spherical particles (diameter 200 μm, density 2500 kg/m^3) represent the behaviour of glass ballotini fluidized by water at ambient conditions. Geometry and physical properties of the system are listed in Table 1. It shall be noted that in order to speed up the computation, lower than realistic contact parameters have been used. Since particle-particle contacts do not play a key role in this fluid-dynamic dominated context, this should allow quicker simulations without seriously affecting the results.

An initial condition is generated by the simulation of a system where the particles are regularly arranged along the system height at sufficient distance to allow movements without immediate contact. The particles are then assigned a random velocity and let fall under gravity, until complete settling is attained. This allows

Table 1. System geometry and physical properties. Water fluidized glass ballotini.

System size (width × height × depth)	1.8 × 8 × 0.02 cm^3
Particle diameter	200 μm
Particle density	2500 kg m^{-3}
Wall and particle Young's modulus	$1 \cdot 10^8$ Pa
Wall and particle Poisson ratio	0.25
Particle-particle and particle-wall restitution coefficient	0.9
Particle-particle and particle-wall friction coefficient	0.3
Fluid density	1000 kg m^{-3}
Fluid viscosity	$1.3 \cdot 10^{-3}$ Pa s
Fluid inlet velocities	0.9,1.2,1.5,4.0 cm s^{-1}
Number of particles	15000
Number of computational cells (width × height × depth)	36 × 100 × 1
Integration time step	$1 \cdot 10^{-5}$ s

producing random packings of the particles similar to the ones obtained in experiments. The so generated initial configuration of the bed is characterized by an average voidage of $\varepsilon_0 = 0.417$ at which minimum fluidization, evaluated using a formula similar to Eq. (2) but valid for particle beds, is for $u = u_{mf}(\varepsilon_0) = 0.68$ mm s^{-1}.

By setting an inlet water velocity of $u_{in} = 1.2$ mm s^{-1}, it is observed that the initially packed bed undergoes a rather homogeneous expansion during the simulation, until a final equilibrium height is reached. Simulations as long as 30 s have been necessary to attain steady state conditions. Visual observation reports a uniformly dense system during expansion, with no tendency towards the formation of bubbles. Under steady-state fluidization, uniform distribution of the particles throughout the system is observed and this voidage homogeneity is found at all the investigated inlet velocities. Steady-state voidage values are reported in Fig. 1.

In the initial seconds of simulation the height of the system undergoes a constant increase with time. In fact, the system is subjected to a sudden change of the inlet velocity from 0 to 1.2 mm s^{-1}, so a voidage shock propagate from the bottom to the top of the bed, with a fairly sharp interface between an upper zone at ε_0 and a lower zone, increasing in thickness, at the new ε, in equilibrium with the new velocity. A

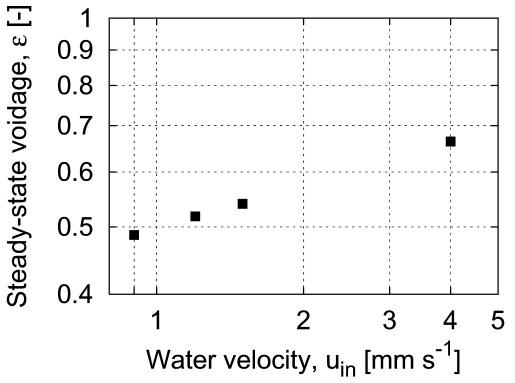

Figure 1. Steady-state voidage versus fluid velocity on a log-log scale.

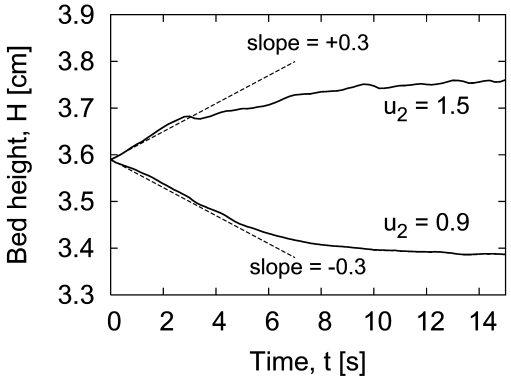

Figure 2. Transient bed height as the velocity is changed from 1.2 to 0.9 and to 1.5 mm s^{-1}. Dashed line represent theoretical slopes (from Eq. (7).

comparison of DEM–CFD simulations and Particle Bed Model (PBM) predictions implies an evaluation of the wave propagation velocities. Kinematic shock propagation velocities can easily be derived by measurements of the transient rise (or drop) of the bed surface after a velocity positive (or negative) step disturbance (Fig. 2). Measurement of the dynamic shock velocities will be attempted in the following section in the case of gas fluidization. Following PBM derivations, the velocity of the rising surface, as a result of the equilibrium conditions varied from (u_1, ε_1) to (u_2, ε_2) is

$$\frac{dH}{dt} = u_2 - u_1 \tag{7}$$

Figure 2 shows the transient position of the bed surface in the simulations, along with the prediction of the initial slope obtained from Eq. (7). Despite the calculations come from significantly different approaches, a very good quantitative agreement is found.

GAS-FLUIDIZED BED

Powders belonging to Group A are usually fine and light particles in which the cohesive forces are not predominant. Porous alumina (density 1000 kg m^{-3}) particles of 70 μm have been considered under air-fluidization. The system geometry and properties are listed in Table 2. Considerations similar to liquid fluidized beds are valid for the material properties of the solids. At this point it is important to remark that the whole analysis will be carried out on a purely hydrodynamic basis, i.e. in the absence of cohesive forces between the particles. An initial condition was generated first. The packed bed state was characterized by a voidage of ε_0 = 0.460, leading to a minimum fluidization velocity of u_{mf} = 3.9 mm s^{-1}.

Following PBM derivations it is possible to predict the transition from homogeneous to bubbling regime by considering the propagation velocities of the kinematic and dynamic waves in the system as the voidage increases from the packed bed state up to 1 (see (10)). The value of ε at which the two velocities are equal determines the condition of critical stability, i.e. it corresponds to the minimum bubbling voidage ε_{mb}. For the air fluidization of alumina the value of the critical voidage is ε_{mb} = 0.543. The equilibrium air velocity is u_{mb} = 8.4 mm s^{-1}.

Starting from a base case with air superficial velocity of 5.0 mm s^{-1}, we ran a set of simulations at various velocities spanning from 4.5 to 12 mm s^{-1}. For each simulation, steady-state spatially averaged voidage and standard deviation have been evaluated. Fig. 3 shows the steady-state voidage values along with error-bars indicating plus/minus two standard deviations. It is shown that relatively small standard deviations are observed below the minimum bubbling condition, whereas zones with significantly different values of the voidage appear as the velocity is increased at 12 mm s^{-1}. It is noteworthy that 9.0 mm s^{-1} is close to the analytical u_{mb}, actually slightly higher, whereas an average voidage of ε = 0.536 is found from post-processing of the results. This shall be explained by the implicit assumption of voidage homogeneity. In fact the relation of u with ε is extremely sensitive to the latter, and, as it is well known, small changes in its value determine significant changes in the corresponding velocity. Therefore, although analytical calculations provide useful approximations, the actual voidage *distribution* influences the real

The 12th International Conference on Fluidization - New Horizons in Fluidization Engineering, pp. 77-81 [2007]

Table 2. System geometry and physical properties. Air fluidized alumina.

System size (width × height × depth)	0.5 × 3 × 0.007 cm^3
Particle diameter	70 μm
Particle density	1000 kg m^{-3}
Wall and particle Young's modulus	$1 \cdot 10^8$ Pa
Wall and particle Poisson ratio	0.25
Particle-particle and particle-wall restitution coefficient	0.9
Particle-particle and particle-wall friction coefficient	0.3
Fluid density	1.205 kg m^{-3}
Fluid viscosity	$1.8 \cdot 10^{-5}$ Pa s
Fluid inlet velocities	4.5, 5.0, 5.5, 6.0, 6.5, 7.0, 9.0, 12.0 cm s^{-1}
Number of particles	10000
Number of computational cells (width × height × depth)	25 × 100 × 1
Integration time step	$5 \cdot 10^{-7}$ s

flow paths and determines an equilibrium velocity that can be slightly different from the calculated value.

Homogeneous distribution of the particles is found for velocities below 9.0 mm s^{-1}, whereas distinct bubbles appear at 12 mm s^{-1}. At the value of 9.0 mm s^{-1}, the bubbling regime is about to establish. The transition between the two regimes is gradual but evident. During homogeneous expansion we are able to investigate on the bed surface velocity at the beginning of the simulation. As in the case of liquid fluidized beds, this value can be easily related to continuity voidage waves travelling across the suspension system. The analytical expression for the surface rising velocity is given by Eq. (7). The transient analysis on the instantaneous bed surface position corresponds to the expected behaviour (Fig. 4), in that the initial slope is graphically equal to the theoretical one. The bed height increases linearly in the first part and eventually reaches the value corresponding to the voidage in equilibrium with the new velocity u_2.

The dynamic wave velocity is reported (10) to be analytically described by the

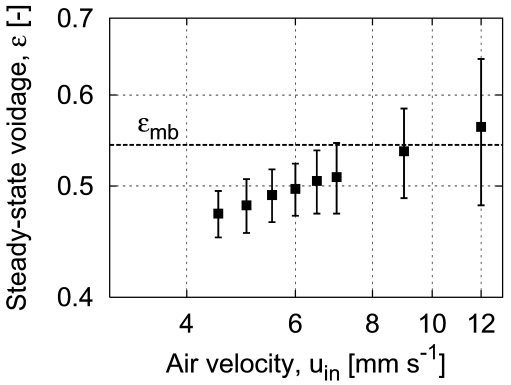

Figure 3. Steady-state spatially averaged voidage values attained at various gas velocities. Error-bars indicate twice the standard deviation.

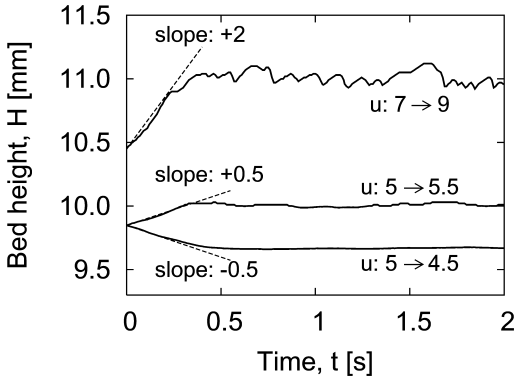

Figure 4. Transient height as the velocity is changed as indicated (in mm s^{-1}). Dashed lines represent theoretical slopes (from Eq. (7)).

following expression

$$u_D = \sqrt{3.2g\,2R(1-\varepsilon_0)(\rho_p - \rho)/\rho_p} \tag{8}$$

In contrast to the kinematic shock, the experimental measurement of u_D is rather difficult. The technique cited in (10) consists of a set of *rain down* experiments, in which a bed of particle is initially packed up against a wire mesh in a fluidization column using a very high fluid velocity. Then, suddenly decreasing the fluid velocity to a value between approximately twice u_{mf} and u_{mf} the particles start detaching, layer after layer, from the plug, showing a fairly neat interface between the detached particles and the ones still stuck. This interface travels along the compressed bed with a velocity that is demonstrated to be that of a dynamic shock. The dynamic wave velocity can be found by extrapolation of the velocities of the shocks measured in experiments in which the bed is subjected to successively decreasing value of the fluid velocity. Precisely, u_D is the travelling velocity of the interface as the fluid velocity tends to u_{mf} (from higher values). Following this procedure, the dynamic shock velocities have been determined for the alumina particles fluidized by air. An initial bed of particles packed against a superior grid was obtained after increasing the gas velocity up to a very high value. The packed bed voidage was ε_0 = 0.455 and the corresponding minimum fluidization velocity is u_{mf} = 3.7 mm s^{-1}. By evaluating the initial height and the time when the top surface was detaching, the interface velocity has been extracted from the simulations and plotted against the excess velocity with respect to the minimum fluidization condition (Fig. 5). An implicit assumption is that u_D is constant during the detachment process, while it has been verified that deviations of about 5% have been found, especially at velocities close to u_{mf}. This is most probably due to the fact that, in these conditions, the interface deforms while travelling and is not as flat as for higher velocities.

The predicted value of the dynamic wave velocity, obtained through a linear fit (Fig. 5), is 37.7 mm s^{-1} and compares well with the theoretical value of 34.6 mm s^{-1} calculated using Eq. (8).

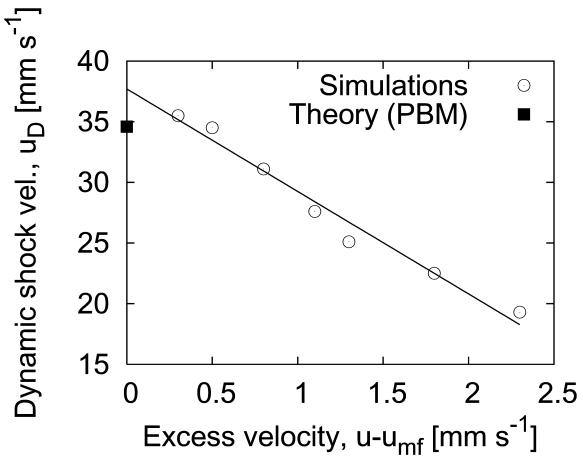

Figure 5. Dynamic shock velocity as a function of the excess fluidization velocity. The symbol at zero represent the theoretical wave velocity (from Eq. (8)). The linear fit (R^2 = 0.9754) presents an intercept of 37.7 mm s^{-1}.

The 12th International Conference on Fluidization - New Horizons in Fluidization Engineering, Art. 81 [2007]

CONCLUSIONS

The simulation capabilities of a DEM-CFD approach have been assessed through representation of the behaviour of a liquid- and gas-fluidized bed. Water fluidized glass ballotini showed a homogeneous expansion in all the investigated range of fluid velocity. Air fluidized fine alumina powder (Group A) showed a transition from homogeneous to bubbling regime around a voidage value in quantitative agreement with the theory of stability of the homogeneously fluidized bed state. In this case, kinematic and dynamic wave propagation velocities have been extracted from the simulations and compared with the theoretical predictions, showing a good agreement.

ACKNOWLEDGEMENT

The authors are grateful to the Italian Ministry of Education, University and Research (MIUR) for its financial support under the Project PRIN 2005 No. 61 (Area: 09).

NOTATION

$\mathbf{a}$	acceleration	t	time
C_D	drag coefficient	u	fluid velocity
$\mathbf{f}$	force	v	particle velocity
$\mathbf{F}_{fp}$	fluid-particle force	V	volume
$\mathbf{g}$	acceleration of gravity	Ω	computational cell volume
H	bed height	χ	empirical parameter in Eq. (2)
m	mass	ε	voidage
p	pressure	ρ	density
R	particle radius	$\boldsymbol{\tau}$	deviatoric stress tensor

Subscripts

0,1,2	initial and subsequent conditions	mb	minimum bubbling
c	contact	mf	minimum fluidization
d	drag	nC	number of contacts
D	dynamic	nP	number of particles in a cell
K	kinematic	p	particle

REFERENCES

1. Cundall, P.A. and Strack, O.D.L. (1979). *Géotechnique*, **29**, 47.
2. Malone, K., Xu, B., Fairweather, M., and Dixon, C. (2005). *Proc. of the 7th World Congress of Chemical Engineering*. Glasgow, UK, P45-017.
3. Chen, C. and Fan, L.-S. (2004). *AIChE Journal*, **50**, 288.
4. Ye, M., van der Hoef, M.A., and Kuipers, J.A.M. (2004). *Powder Technology*, **139**, 129.
5. Ye, M., van der Hoef, M.A. and Kuipers, J.A.M. (2005). *Chemical Engineering Science*, **60**, 4567.
6. Pandit, J.K., Whang, X.S. and Rhodes, M.J. (2005). *Powder Technology*, **160**, 7.
7. Foscolo, P.U. and Gibilaro, L.G. (1987). *Chemical Engineering Science*, **42**, 1489.
8. Di Renzo, A. and Di Maio, F.P. (2005). *Chemical Engineering Science*, **60**, 1303.
9. Di Felice, R. (1994). *International Journal of Multiphase Flow*, **20**, 153.
10. Gibilaro, L.G. (2001). *Fluidization-dynamics*. Butterworth-Heinemann, Oxford.